Direct observation of the bandwidth-disorder induced variation of charge/orbital ordering structure in $RE_{0.5}(Ca_{1-y}Sr_y)_{1.5}MnO_4$

2007 J. Phys.: Condens. Matter 19 172203

(http://iopscience.iop.org/0953-8984/19/17/172203)

IOP FTC

IOP PUBLISHING JOURNAL OF PHYSICS: CONDENSED MATTER

J. Phys.: Condens. Matter **19** (2007) 172203 (8pp) doi:10.1088/0953-8984/19/17/172203

FAST TRACK COMMUNICATION

Direct observation of the bandwidth-disorder induced variation of charge/orbital ordering structure in $RE_{0.5}(Ca_{1-y}Sr_y)_{1.5}MnO_4$

X Z Yu[1,2], T Arima[1,3], Y Kaneko[1,4], J P He[1], R Mathieu[1], T Asaka[2], T Hara[2], K Kimoto[2], Y Matsui[2] and Y Tokura[1,4,5,6]

[1] Spin Super Structure Project, Exploratory Research for Advanced Technology (ERATO), Japan Science and Technology Agency, Tsukuba 305-8562, Japan
[2] Advanced Electron Microscopy Group, National Institute for Materials Science, Tsukuba, 305-0044, Japan
[3] Institute of Multidisciplinary Research for Advanced Materials, Tohoku University, Sendai 980-8577, Japan
[4] Multiferroics Project, Exploratory Research for Advanced Technology, Japan Science and Technology Agency, Tsukuba, 305-8562, Japan
[5] Correlated Electron Research Center (CERC), National Institute of Advanced Industrial Science and Technology (AIST), Tsukuba 305-8562, Japan
[6] Department of Applied Physics, University of Tokyo, Tokyo 113-8656, Japan

E-mail: Yu.xiuzhen@nims.go.jp

Received 10 March 2007
Published 16 April 2007
Online at stacks.iop.org/JPhysCM/19/172203

Abstract

Changes in the charge/orbital ordering (CO/OO) structure with the bandwidth of the e_g band and quenched disorder were investigated in doped manganites $RE_{0.5}(Ca_{1-y}Sr_y)_{1.5}MnO_4$ (RE = Pr, Eu) with a single-layer perovskite structure. A systematic study of the modulation structure associated with the CO/OO phase demonstrated that the long-range commensurate structure changes to a short-range incommensurate structure with increasing Sr content through the enhancement of the bandwidth and quenched disorder in these systems. At the same time, the transition temperature of CO/OO ($T_{CO/OO}$) decreases. Changes in structure and $T_{CO/OO}$ with different A-site combinations reveal that the CO/OO phase is strongly suppressed by the widening of the e_g band and the stronger quenched disorder in these layered manganites.

(Some figures in this article are in colour only in the electronic version)

1. Introduction

Recent studies [1–4] on doped manganites $RE_{1-x}AE_xMnO_3$ (RE: a rare earth element; AE: an alkaline earth element) with a perovskite structure have revealed that the competition

between the ferromagnetic (FM) phase and the charge/orbital ordering (CO/OO) phase yields the colossal magnetoresistance (CMR) phenomenon. In the FM phase, e_g electrons on Mn^{3+} are mobile and their orbitals are disordered. In the CO/OO phase, ordering of Mn^{3+}/Mn^{4+} accompanied by a simultaneous ordering of e_g orbitals with $3x^2 - r^2$ and $3y^2 - r^2$ (where x and y are spatial coordinates) makes orbital stripes in the ab plane. Corresponding to these periodic stripes, a modulation structure is created. In these manganite systems, the stabilities of the FM phase and the CO/OO phase are affected by the effective one-electron bandwidth of the e_g band (W) and the presence of quenched disorder [4–6]. W is dependent on the lattice distortion that relates to the average ionic radius (r_A) of the A-site cations, $r_A = \sum_i x_i r_i$, where x_i and r_i are the fractional occupancy and the effective ionic radius of the A-site cations, respectively. As r_A increases, the Mn–O–Mn bond angle decreases, and the bandwidth W increase results in a stable FM phase [4]. On the other hand, the quenched disorder is associated with a temperature-independent atomic-scale local inhomogeneity which induces randomness in potential energy, transfer energy, exchange interaction, and so on [2]. The intrinsic inhomogeneity in these doped manganites is caused by the unavoidable random chemical substitution of AE for RE. This randomness can be evaluated from the variance of the A-site ionic radii, $\sigma = (\sum_i x_i r_i^2 - r_A^2)^{1/2}$ [7–9]. The CO/OO phase, as well as the FM phase, collapses as σ increases. The significant effect of quenched disorder on CO/OO in doped manganites $RE_{1-x}AE_xMnO_3$ ($x = 0.45$) was revealed by resistivity and ac susceptibility measurements [4]. The electronic phase diagram in the plane of r_A and σ indicates that a long-range CO/OO exists in $RE_{0.55}Ca_{0.45}MnO_3$, which has a relatively narrow bandwidth and weak quenched disorder. By replacing Ca with Sr, the CO/OO can be suppressed and the FM phase will develop because of the increase in W. In contrast with the $RE_{1-x}AE_xMnO_3$ system, in the single-layer manganites A_2MnO_4 (where A is composed of RE and AE elements), the FM correlation is completely suppressed [10] and the insulating phase is dominant since each MnO_2 layer (in-plane) is isolated by the (RE or AE) O blocks. The CO/OO phase is expected to be stabilized in this system. We have reported [11] that the long-range CO/OO phase exists in single-layer manganites $Pr_{1-x}Ca_{1+x}MnO_4$ over a wide range of hole doping levels x. For $x = 0.5$ (i.e. $Pr_{0.5}Ca_{1.5}MnO_4$), with a relatively narrow bandwidth and weak quenched disorder, the commensurate modulation structure associated with the long-range CO/OO was observed. In contrast to this behaviour, only a short-range CO/OO has been observed in $Pr_{0.5}Sr_{1.5}MnO_4$ [12]. However, it is not clear whether the sharp contrast is mainly attributed to the difference in bandwidth or in quenched disorder. To understand the role of bandwidth and quenched disorder in the layered manganites, we thus studied the CO/OO structure in $Pr_{0.5}(Ca_{1-y}Sr_y)_{1.5}MnO_4$ and $Eu_{0.5}(Ca_{1-y}Sr_y)_{1.5}MnO_4$ single crystals systematically by changing the Sr concentration, which affects the r_A and σ of these systems. The variations in the CO/OO structure, e.g. the variation in the CO/OO coherence length and modulation wavenumber with the A-site combinations, were investigated in detail by means of transmission electron microscopy (TEM) [11–15]. Changes in the transition temperature of CO/OO ($T_{CO/OO}$) with Sr concentration were also studied.

2. Experimental results and discussion

Single crystals of $RE_{0.5}(Ca_{1-y}Sr_y)_{1.5}MnO_4$ (RE = Pr, Eu) with various Sr concentrations y were grown using the floating-zone melt method [9]. The phase purity and cation concentrations were checked by using powder x-ray diffraction and inductively coupled plasma (ICP) atomic emission spectroscopy, respectively. Electron-transparent thin samples were prepared by mechanical polishing and subsequent argon-ion thinning with an acceleration voltage of 4 kV at room temperature. Selected-area electron diffraction (SAED) patterns and

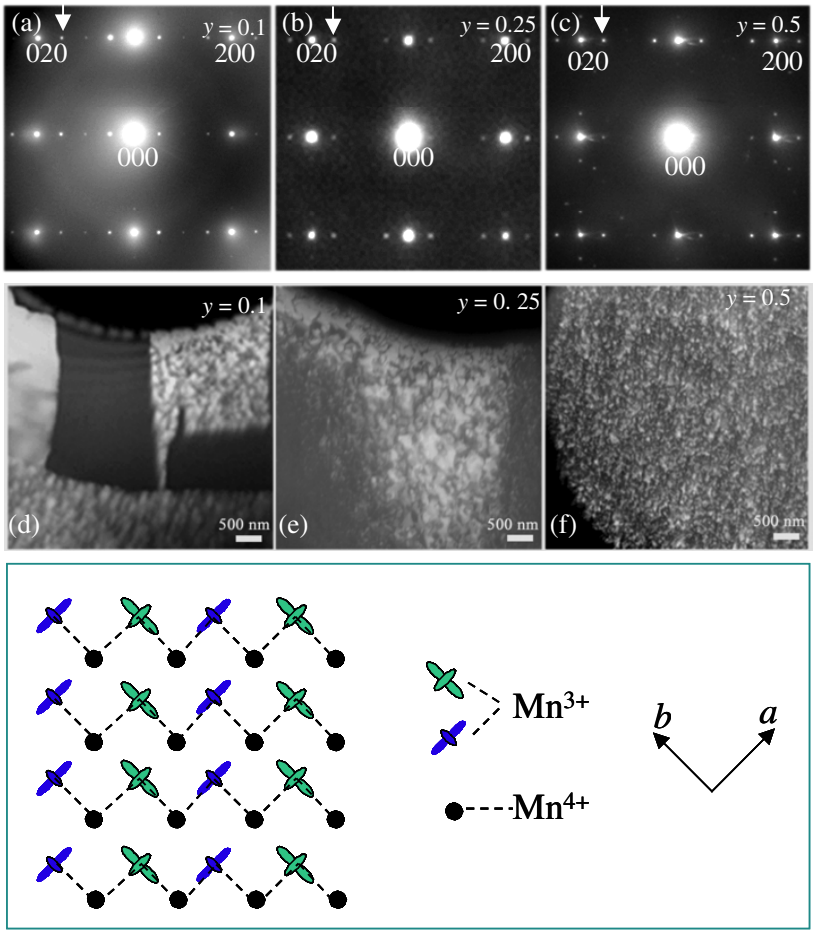

Figure 1. (a)–(c) The [001]-zone electron diffraction patterns and (d)–(f) corresponding dark-field images associated with CO/OO domain structures of $Pr_{0.5}(Ca_{1-y}Sr_y)_{1.5}MnO_4$ at 83 K. Indices are based on a tetragonal K_2NiF_4 structure with lattice parameters of $a \sim 3.8$ Å and $c \sim 11.8$ Å. The dark-field images obtained by using the SL spots $(\delta, 2+\delta, 0)$ (marked by white arrows) reveal the CO/OO domain structures which change with the Sr content y. Here, δ is the wavenumber of the superstructure associated with the CO/OO. The bottom panel is a schematic diagram for $d_{3x^2-r^2}/d_{3y^2-r^2}$-type CO/OO.

dark-field (DF) images were obtained by using two transmission electron microscopes (Hitachi HF-3000S and HF-3000L), both equipped with a cold-field emission gun and a liquid nitrogen cooling holder.

Figure 1 shows the SAED patterns and corresponding DF images, as captured in the *ab* plane of $Pr_{0.5}(Ca_{1-y}Sr_y)_{1.5}MnO_4$ for various Sr concentrations at 83 K. Superlattice (SL) spots are clearly observed in the [001]-zone SAED patterns. For simplicity, the indices of the fundamental spots are based on the tetragonal setting with $a_t \times a_t \times c_t$ (a_t, c_t: lattice parameters of tetragonal K_2NiF_4 structure). These SL spots reflect the modulation structure of CO/OO more precisely, the $d_{3x^2-r^2}/d_{3y^2-r^2}$-type CO/OO, in which the e_g orbitals on Mn^{3+} stripes with zig-zag $3x^2 - r^2$ and $3y^2 - r^2$ arrangements alternate with the Mn^{4+} stripes, as depicted in the lower panel of figure 1. Analyses of the SAED patterns revealed that the SL

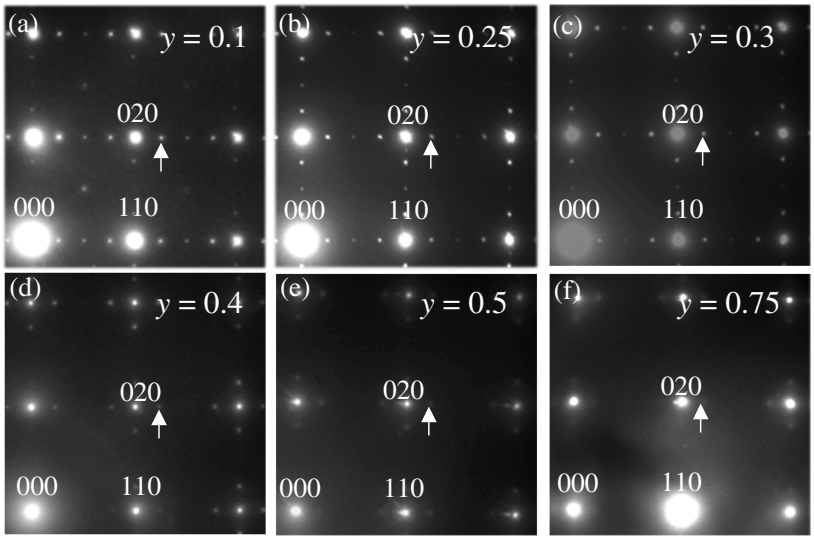

Figure 2. The [001]-zone electron diffraction patterns of $Eu_{0.5}(Ca_{1-y}Sr_y)_{1.5}MnO_4$ with various Sr content ($y = 0.1$–0.75) at 83 K. Indices are based on a tetragonal K_2NiF_4 structure with lattice parameters of $a \sim 3.8$ Å and $c \sim 11.8$ Å.

spots become broader with increasing Sr concentration. Only diffuse scattering was observed for samples with $y > 0.5$ (not shown). Figures 1(d) and (f) show the corresponding DF images that were obtained for the SL spots in figures 1(a) and (c) (indicated by white arrows). These DF images reflect the microstructures of the CO/OO domains in these crystals. The bright/dark band-shaped domains exhibit the CO/OO twins with two perpendicular directions. In each bright area corresponding to a single CO/OO domain, one can see many grains separated by grey curved lines, indicating antiphase boundaries (APB) due to the local disarrangements of $3x^2 - r^2$ and $3y^2 - r^2$ orbitals. For $y = 0.1$, the CO/OO domain size typically ranges from hundreds of nanometres to several micrometres. The domain size decreases with increasing y. Only nanometre-sized CO/OO clusters are evident for $y = 0.5$.

Figure 2 shows the SAED patterns in the *ab* plane for $Eu_{0.5}(Ca_{1-y}Sr_y)_{1.5}MnO_4$ at 83 K. Similar to the $Pr_{0.5}(Ca_{1-y}Sr_y)_{1.5}MnO_4$ crystals, SL spots associated with the $d_{3x^2-r^2}/d_{3y^2-r^2}$-type CO/OO are observed in the [001]-zone SAED patterns. The changes in the sharpness of the SL spots with increasing Sr concentration are such that the sharp SL spots for $y \leqslant 0.4$ become diffuse scattering for $y > 0.4$. Compared with the $Pr_{0.5}(Ca_{1-y}Sr_y)MnO_4$ case, the long-range CO/OO of $Eu_{0.5}(Ca_{1-y}Sr_y)_{1.5}MnO_4$ collapsed with fewer Sr substitutions. Changes in the CO/OO structure of $Eu_{0.5}(Ca_{1-y}Sr_y)_{1.5}MnO_4$ were determined by studying the variations in the coherence length and modulation wavenumber (δ) with Sr concentration. Figure 3 shows the y dependence of δ and the half width at half maximum (HWHM) of $(\delta, 2+\delta, 0)$ spots. The HWHM is inversely proportional to the coherence length. The HWHM increases marginally with Sr concentration until $y = 0.4$, and rapidly increases from $y = 0.4$ to 0.5. This indicates that the long-range CO/OO for $y < 0.4$ crystals changes into short-range CO/OO for $y > 0.4$. The modulation wavenumber varied from commensurate for $y \leqslant 0.25$ to incommensurate for $y > 0.25$.

To obtain direct images of the CO/OO domain structure, the DF images were observed below $T_{CO/OO}$. Figure 4 shows the DF images in the *ab* plane for $Eu_{0.5}(Ca_{1-y}Sr_y)_{1.5}MnO_4$ crystals at 83 K. These images were obtained from the SL spots indicated by the white arrows

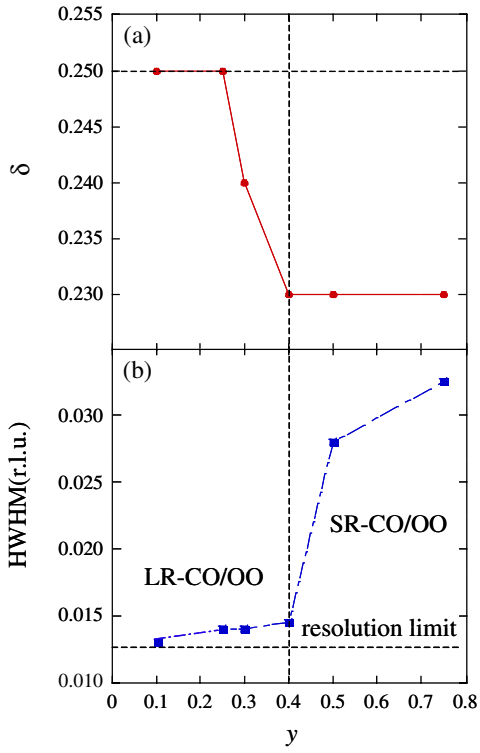

Figure 3. (a) Modulation wavenumber δ and (b) half width at half maximum (HWHM) of the $(\delta, 2+\delta, 0)$ SL spots marked by the white arrows in figure 2 which are associated with the CO/OO domain structures of $RE_{0.5}(Ca_{1-y}Sr_y)_{1.5}MnO_4$ (RE = Pr, Eu) for various Sr content y, at 83 K.

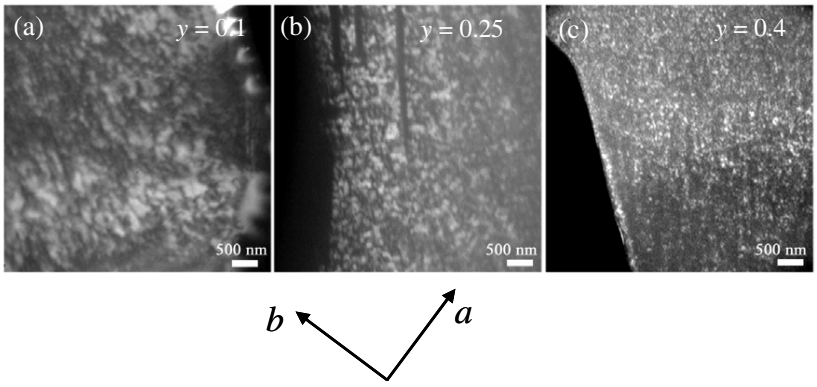

Figure 4. Dark-field images associated with the CO/OO domain structures of $Eu_{0.5}(Ca_{1-y}Sr_y)_{1.5}MnO_4$ for various Sr content y, at 83 K. These images were obtained by using SL spots $(\delta, 2+\delta, 0)$ indicated by the white arrows in figure 2 and they reveal the CO/OO domain structures.

in figure 2. Short-range CO/OO with nanometre-size domains are visible at $y = 0.4$. Here, it is noteworthy that long-range CO/OO with sub-micrometre-size domains is observed in the RE = Pr crystal at $y = 0.25$ (in figure 1(e)) with the same r_A and smaller σ. (The values of

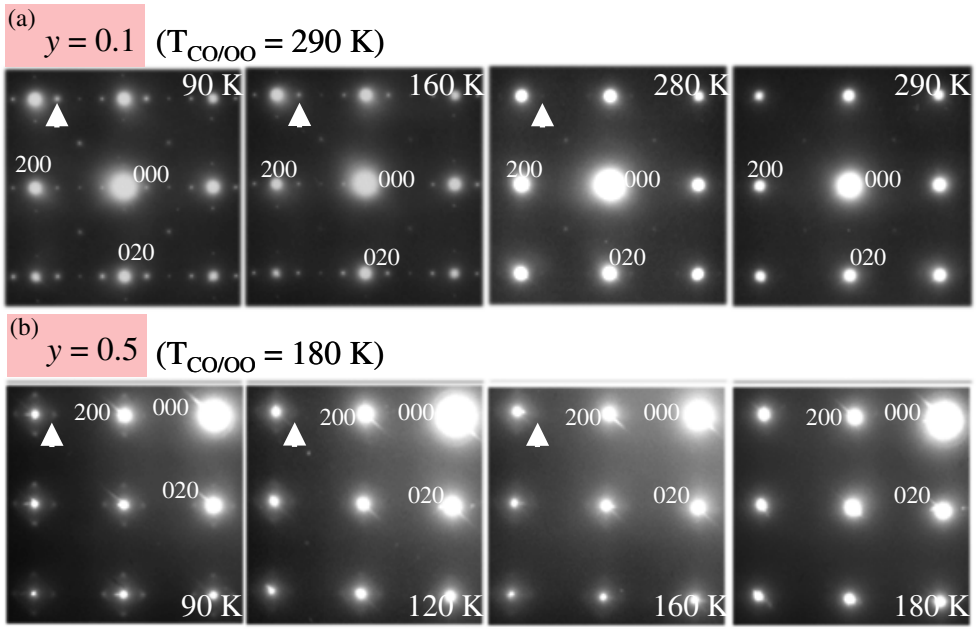

Figure 5. Temperature dependence of the [001]-zone electron diffraction patterns in $Eu_{0.5}(Ca_{1-y}Sr_y)_{1.5}MnO_4$ for (a) $y = 0.1$ and (b) $y = 0.5$.

r_A and σ are presented in figure 6.) This difference implies that the stability of CO/OO in the layered manganites decreases with increasing variance σ in the A-site ionic radii.

Figures 5(a) and (b) show the temperature dependence of the SAED patterns of $Eu_{0.5}(Ca_{1-y}Sr_y)_{1.5}MnO_4$ for $y = 0.1$ and $y = 0.5$, respectively. The SL spots associated with the long-range CO/OO at $y = 0.1$ vanish at 290 K. For $y = 0.5$, the diffusion scatterings associated with the short-range CO/OO disappear at above 180 K. Figure 6 shows the electronic phase diagram of $RE_{0.5}(Ca_{1-y}Sr_y)_{1.5}MnO_4$ (RE = Pr or Eu) in the plane of the average ionic radius r_A and the variance in the A-site ionic radius σ, obtained by systematically investigating the modulation structures in these crystals for various Sr concentrations at various temperatures. The red and light green curves, respectively, represent the temperatures at which long-range and short-range orbital order appear. When r_A is fixed, $T_{CO/OO}$ decreases with increasing σ. For example, the $T_{CO/OO}$ is about 240 K for the RE = Pr crystal of $y = 0.5$ for which σ^2 is $\sim 2.6 \times 10^{-3}$. However, the $T_{CO/OO}$ is about 160 K for the RE = Eu crystal of $y = 0.4$ for which σ^2 is $\sim 5.5 \times 10^{-3}$. On the other hand, when σ is fixed, for the RE = Eu crystal of $y = 0.3$ and the RE = Pr crystal of $y = 0.5$, $T_{CO/OO}$ decreases from 220 to 180 K with increasing r_A. These results mean that the CO/OO in these systems is suppressed either by the larger variance in the A-site ionic radii or by the larger averaged ionic radius of the A-site. Changes in the CO/OO structures for different A-site combinations have been found to affect the macroscopic properties such as magnetization and electrical resistivity. For example, the long-range antiferromagnetic spin ordering in $Eu_{0.5}(Ca_{1-y}Sr_y)_{1.5}MnO_4$ for $y < 0.4$ is replaced by the spin-glass state for $y > 0.4$ [9], in which only short-range incommensurate CO/OO exists. As the quenched disorder becomes stronger, the ordering of e_g orbitals on Mn^{3+} is suppressed, yielding a spin-glass state [16]. In other words, the short-range nature of antiferromagnetic spin ordering for $y > 0.4$ is strongly correlated to the collapse of the e_g orbital ordering [11].

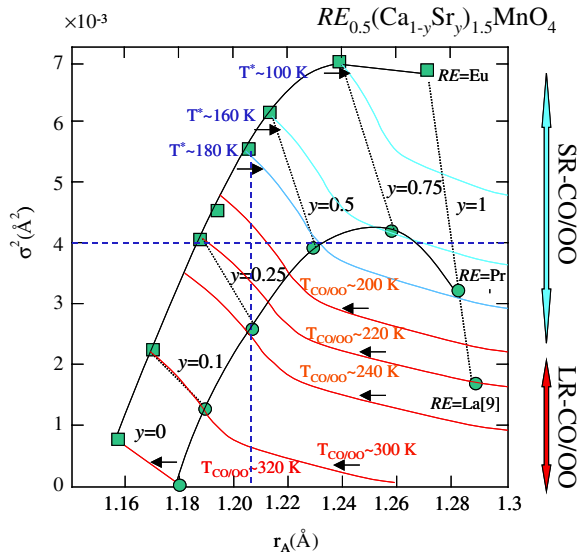

Figure 6. Electronic phase diagram of $RE_{0.5}(Ca_{1-y}Sr_y)_{1.5}MnO_4$ in the plane of the average ionic radius and the variance in A-site ionic radii. Solid and dotted lines connect the crystals with the same RE cation and Sr content y, respectively. Red and light green lines show the contour lines of $T_{CO/OO}$ and T^*, respectively. $T_{CO/OO}$ and T^* indicate the transition temperature of the long-range CO/OO and the crossover temperature of short-range CO/OO, respectively.

In conclusion, by observing the CO/OO structures in $Pr_{0.5}(Ca_{1-y}Sr_y)_{1.5}MnO_4$ and $Eu_{0.5}(Ca_{1-y}Sr_y)_{1.5}MnO_4$ crystals directly, we have demonstrated that the CO/OO structure in single-layer manganite systems is strongly correlated to the bandwidth of the e_g band and the quenched disorder caused by the mismatch of the ionic size of the A-site. Substituting Sr for Ca in $RE_{0.5}Ca_{1.5}MnO_4$ (RE = Pr or Eu) changes the CO/OO correlation from long-ranged to short-ranged, and the modulation wavevector from commensurate to incommensurate. The enhancement of the bandwidth and the quenched disorder strongly suppress the CO/OO as well as the spin ordering in layered manganites. This effect gives us with insight into the phase control mechanism in such materials.

We thank Drs M Uchida and T Nagai for valuable discussions, and Mr C Tsuruta for technical support. This work was supported partly by the Nanotechnology Support Project of the Ministry of Education, Culture, Sports, Science and Technology (MEXT), Japan.

References

[1] Tokura Y (ed) 2000 *Colossal Magnetoresistive Oxide* (London: Gordon and Breach)
[2] Tokura Y 2006 *Rep. Prog. Phys.* **69** 797
[3] Tomioka Y and Tokura Y 2002 *Phys. Rev.* B **66** 104416
[4] Tomioka Y and Tokura Y 2004 *Phys. Rev.* B **70** 014432
[5] Moreo A, Mayr M, Feiguin A, Yunoki S and Dagotto E 2000 *Phys. Rev. Lett.* **84** 5568
[6] Motome Y, Furukawa N and Nagaosa N 2003 *Phys. Rev. Lett.* **91** 167204
[7] Rodriguez-Martinez L M and Attfield J P 1998 *Phys. Rev.* B **54** R15622
[8] Rodriguez-Martinez L M and Attfield J P 2000 *Phys. Rev.* B **63** 024424
[9] Mathieu R, Uchida M, Kaneko Y, He J P, Yu X Z, Kumai R, Arima T, Tomioka Y, Asamitsu A, Matsui Y and Tokura Y 2006 *Phys. Rev.* B **74** 020404

[10] Larochelle S, Mehta A, Lu L, Mang P K, Vajk O P, Kaneko N, Lynn J W, Zhou L and Greven M 2005 *Phys. Rev.* B **71** 024435
[11] Yu X Z, Arima T, Kaneko Y, He J P, Uchida M, Asaka T, Nagai T, Kimoto K, Matsui Y and Tokura Y *Phys. Rev.* B to be published
[12] Uchida M, Mathieu R, He J P, Kaneko Y, Asamitsu A, Kumai R, Tomioka Y, Matsui Y and Tokura Y 2006 *J. Phys. Soc. Japan* **75** 053602
[13] Mori S, Chen C H and Cheong S W 1998 *Nature* **392** 473
[14] Nagai T, Kimura T, Yamazaki A, Asaka T, Kimoto K, Tokura Y and Matsui Y 2002 *Phys. Rev.* B **65** 060405(R)
[15] Asaka T, Yamada S, Tsutsumi S, Tsuruta C, Kimoto K, Arima T and Matsui Y 2002 *Phys. Rev. Lett.* **88** 097201
[16] Mathieu R, Akahoshi D, Asamitsu A, Tomioka Y and Tokura Y 2004 *Phys. Rev. Lett.* **93** 227202